Nonlinear-dynamics theory of up-down transitions in neocortical neural networks

Maryam Ghorbani,[1] Mayank Mehta,[1,2,3,4] Robijn Bruinsma,[1] and Alex J. Levine[1,5]

[1]*Department of Physics and Astronomy, University of California, Los Angeles, Los Angeles, California 90095-1547, USA*

[2]*Department of Neurology, Department of Neurobiology, University of California, Los Angeles, Los Angeles, California 90095-1547, USA*

[3]*Integrative Center for Learning and Memory, University of California, Los Angeles, Los Angeles, California 90095-1547, USA*

[4]*Keck Center for Neurophysics, University of California, Los Angeles, Los Angeles, California 90095-1547, USA*

[5]*Department of Chemistry and Biochemistry, University of California, Los Angeles, Los Angeles, California 90095-1547, USA*

(Received 7 July 2011; revised manuscript received 30 November 2011; published 13 February 2012)

The neurons of the neocortex show ∼1-Hz synchronized transitions between an active up state and a quiescent down state. The up-down state transitions are highly coherent over large sections of the cortex, yet they are accompanied by pronounced, incoherent noise. We propose a simple model for the up-down state oscillations that allows analysis by straightforward dynamical systems theory. An essential feature is a nonuniform network geometry composed of groups of excitatory and inhibitory neurons with strong coupling inside a group and weak coupling between groups. The enhanced deterministic noise of the up state appears as the natural result of the proximity of a *partial synchronization transition*. The synchronization transition takes place as a function of the long-range synaptic strength linking different groups of neurons.

DOI: 10.1103/PhysRevE.85.021908 PACS number(s): 87.19.L−, 05.45.−a, 87.18.Sn

I. INTRODUCTION

The theory of dynamical systems has been widely applied to analyze the activity of neurons. A variety of simple model equations that describe the electrical potential and ionic currents associated with the firing of a neuronal action potential spike exhibit a form of *bifurcation* [1]. Most bifurcation types possible for two-component dynamical systems have been observed for different types of neurons in different sections of the brain [2]. The model equations are enormously simplified but the bifurcation classification incorporates general mathematical principles that have more general validity than the equations themselves. The application of dynamical systems theory to *networks* of coupled neurons is currently a very active area of research, in particular, in the context of *synchronization* between networks. Simple neural circuits, such as the one that regulates the breathing rhythm, can be readily analyzed, again by applying the methods of dynamical systems theory to simplified equations [2]. However, analyzing the functionally complex neural circuitry of the cortex is obviously much more challenging. A full theory of cortical neural dynamics should, for example, address far-reaching questions such as the nature of computation executed by spike-timing.

In this paper, we focus instead on the application of dynamical systems theory to collective neural activity inside the cortex section of the brain. An important and common way to characterize the collective activity of the cortex is presented by the electroencephalograph (EEG). An EEG records voltage fluctuations [3] measured on the surface of the skull. Similar signals, called *local field potentials* (LFPs), are measured by microwires inserted into the cortex. EEG and LFP recordings reflect the average activity of a large ensemble ($>10^4$) of neurons surrounding the measurement sites. The signals typically span a frequency range between 0.1 and 300 Hz with a spectral power that increases with decreasing frequency [4].

A striking feature of cortical EEGs and LFPs recorded during slow-wave sleep and anesthesia is regular, large-scale oscillations with a low-frequency range (0.5–2 Hz) and large amplitude (∼1 mV in EEG). They are known as delta oscillations or slow-wave-sleep (SWS) oscillations [5]. The oscillations are coherent across large parts of the cortex and can also be seen in measurements of the membrane potentials of individual neurons [5–7]. Figure 1 shows an example of an intracellular recording of the membrane potential of a single neuron (from Ref. [8]) taken during a period of slow EEG oscillations.

The recording shows that the membrane potential of an individual neuron undergoes repetitive transitions from a quiescent "down" state to a noisy "up" state with a number of spikes. The *resting potential* of a neuron with respect to the surrounding extracellular fluid is around −70 mV. During a down state, a neuron has a membrane potential a few mV below this resting potential and is said to be *hyperpolarized*. Next, if the cell is *depolarized* beyond a threshold of around −55 mV, it will start to fire action potentials (∼100-mV amplitude, ∼1-ms duration) that will travel down the axon. Figure 1 shows that during an up state, a cell occasionally fires an action potential. As shown in Fig. 2, the action potentials, also known as spikes, travel from the cell body ("soma") down the axon to another neuron.

The terminals of the axon are connected by *synaptic junctions* to the *dendrites* of the other neuron (see the inset of Fig. 2). If the initial neuron was excitatory, then the signal has a depolarizing effect, known as an excitatory postsynaptic potential (EPSP). If the initial neuron was inhibitory, then the signal typically has a hyperpolarizing effect, known as an inhibitory postsynaptic potential (IPSP). The total dendritic input determines whether or not the membrane potential of the second neuron will be sufficiently depolarized for it to reach spiking threshold [5]. In a well-connected network of excitatory neurons, positive feedback between different excitatory neurons would produce a burst of action potential firings with a frequency in the 10–100 Hz range. In the up state this does not happen: The (mean) membrane potential remains a few mV *below* the firing threshold and, on average, a neuron will fire at most one action potential during an up state [8]. Control of the level of positive feedback is clearly a necessary feature of up states.

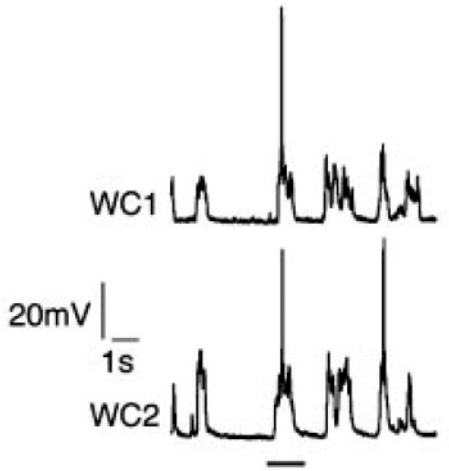

FIG. 1. Whole cell (WC) recording from Ref. [8] of the membrane potential of layer 2/3 pyramidal neurons of a rat. The up-down state oscillations have an average period of about 1 s. The "up" states have a mean amplitude of about +20 mV relative to the membrane potential in the "down" state and they show noisy fluctuations due to a rapid barrage of postsynaptic potentials. In the less noisy "down" states, the neurons are hyperpolarized with a mean potential of −71 mV. The number of action potentials fired by a neuron per up state is typically small, on the order of one. For example, in the lower trace (WC2), we see a single action potential (narrow spike) produced during the second and fourth of the five up states shown.

The repeated cycling between the up-state and down-state potentials is known as up-down state (UDS) oscillations [4]. Under the influence of several anesthetics and during the slow-wave sleep, large-amplitude, 0.5–2 Hz oscillations are present in the EEG in many species including humans, primates, and rodents. These oscillations can also be seen in the neocortical LFP reflecting synchronous changes in the membrane potentials of large neuronal ensembles. During these slow oscillations the neural activity, such as the membrane potential and spiking probability, exhibit bistability such that large ensembles of neurons synchronously make transitions between a more depolarized and more active up state, and a less depolarized and less active down state [5,10]. All types of neurons in the neocortex, including the excitatory and inhibitory neurons' membrane potentials, show virtually synchronous transitions. In other words, excitatory and inhibitory neurons become more active in the up state and less active in the down state [11–13].

Due to their reliable synchrony across many brain areas and neural types, the up-down state transitions have been used to probe the functional connectivity and dynamics of cortical circuits. They could explain some amount of variability of neural responses to stimuli [8,14–16]. Further, it is believed that during the UDS the neocortex and hippocampus interact to facilitate the long-term consolidation of recently formed memories [17–26]. Early studies described the UDS in terms of the membrane potential of excitatory neurons. Later studies showed that during UDS, the spiking probabilities of both excitatory and inhibitory neurons changes synchronously. Hence, UDS can also be detected using the firing rates of large ensembles of neurons [27–30], which results in concomitant two-state oscillations in the LFP [19,21,31,32].

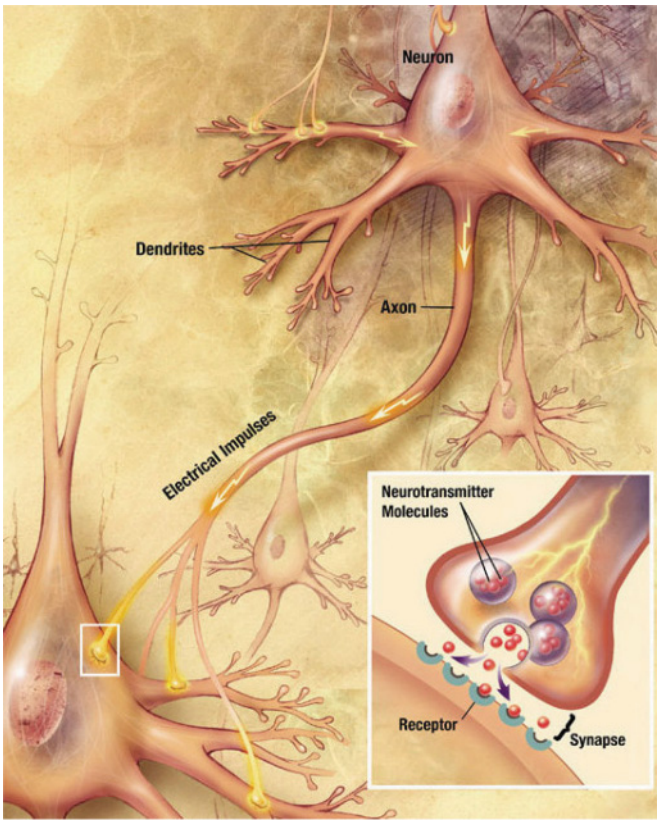

FIG. 2. (Color online) Drawing of a pair of neurons. When the membrane potential of the body ("soma") of the neuron at the top exceeds the firing threshold, an action potential is generated that travels along the axon of the first neuron to the dendrites of the second neuron. Inset: A synaptic junction between an axonal terminal of one cell and the dendrite of a second neuron. When the electrical signal reaches the terminal, neurotransmitters are released into the synaptic cleft and they bind with neuroreceptors in the postsynaptic neuron. This generates an excitatory postsynaptic potential (EPSP) that is depolarizing if the signal comes from an excitatory neuron and an inhibitory postsynaptic potential (IPSP) that is typically hyperpolarizing if it comes from an inhibitory neuron. (Image from Ref. [9].)

Observations on UDS oscillations can be summarized as follows.

(i) In the active (up) state of the cycle, individual neocortical neurons fire rarely, with a typical rate that is less than 1 Hz [8]. The cell body receives from its dendrites an avalanche of EPSPs and IPSPs, which explains the noise in the up state in Fig. 1. The mean membrane potential of the neuron remains somewhat below threshold in the up state, as already mentioned [8]. One of the questions we will address is how membrane potentials can be regulated in a robust way to lie just below the firing threshold.

(ii) In the less active (down) state, the membrane potential of all neuron types is in a prolonged hyperpolarized state with little evidence of EPSPs and IPSPs [5,8]. Neurons rarely fire a spike during the down state. Thus the membrane potential is essentially biphasic, shuttling between two values during the up-down states.

(iii) The up-state activity is regulated by the inhibitory neurons. Pharmacological reduction in the level of inhibition

results in increased spiking [8]. Complete suppression of inhibition results in an up state state with no up-down state and almost continuous spiking.

(iv) The UDS oscillations are synchronous over large portions of the cortex [8]. The duration of the up state and the oscillation period show significant variability from cycle to cycle.

The precise mechanism(s) that terminates an up state after about 1 s has not been completely determined. The candidate mechanism we focus on here is *dendritic spike frequency adaptation* (DSFA) [33,37]: Incoming action potentials produce an increase in the outward conductance of the dendritic membrane. Experiments report that spike frequency adaptation is shown by virtually all the cortical excitatory neurons, but rarely by the inhibitory neurons. This increased conductance, which may be due to activation of K^+ channels or to a local increase of Ca^{2+}, reduces the ability of the dendritic synaptic junctions of excitatory neurons to generate postsynaptic potentials. DSFA may also be due to the depletion of neurotransmitters in the synaptic clefts.

The UDS oscillations pose a puzzle for a dynamical systems description: They combine collective, highly synchronized regularity with pronounced noise in individual neurons. This switching between up and down states appears not to be externally regulated, which would have been the simplest explanation. Qualitatively similar slow oscillations—although of lower frequency—are also seen *in vitro* in isolated, small ($<mm^2$) slices of the neocortex [6]. For the same reason, the up-state noise is also of an intrinsic nature: Individual neurons are essentially deterministic so the noise, as the up-down state switching, must be a collective property of an ensemble of neurons. Simple models of coupled oscillatory networks report that when the coupling strength is increased, one encounters synchronization through phase locking, as exhibited, for example, by the Kuramoto Model [2,38]. It is difficult to see, however, how one can reconcile the deterministic noise present during the up states with the regularity of the collective switching between the up and down states.

In this paper we present a simple theoretical framework for up-down state dynamics of cortical neural circuits consistent with the features (i)–(iv) listed above. The model is based on DSFA but does not rely on any detailed properties of DFSA [37]. We only assume that (i) synaptic activity in the up state progressively reduces the ability of excitatory (but not inhibitory) neurons to respond to depolarizing synaptic inputs, resulting in the termination of the up state, and (ii) that during the down state, a separate process, such as the activity of Ca^{2+} pumps, slowly restores the ability of a neuron to respond to synaptic input. This results in a gradually increased excitability of the network and an eventual transition to the up state.

There are several possible sources of such adaptation: synaptic, somatic, and dendritic. *In vitro* studies show that all three mechanisms are present in the excitatory neurons. There is little evidence that these three occur in a majority of neocortical inhibitory neurons. This unequal short-term dynamics is the key ingredient responsible for the termination of up states in our model. We believe that all three of them can contribute to this process. Further, given the very low firing rates of excitatory neurons ($\sim$1 Hz), excitatory neurons will fire about one spike per up state, which would not result in a substantial amount of synaptic and somatic adaptation. However, thousands of excitatory inputs terminate on the dendrites. The dendrites of excitatory neurons have voltage-gated channels, many of which are similar to those in the soma, such as the voltage-gated potassium channels, that are responsible for spike frequency adaptation. Hence, we hypothesize that the summation of a large number of excitatory inputs on excitatory neurons' dendrites results in the depolarization of dendrites in the up state, which is likely to engage the dendritic spike frequency adaptation mechanism. The inhibitory synapses mostly terminate on the soma so the dendritic mechanisms would not influence much the inhibitory-inhibitory (I-I) and inhibitory-excitatory (E-I) synapses. Hence we hypothesize that the dendrites would be far more active than either the synapses or the soma in the adaptation of the excitability of the excitatory but not the inhibitory neurons. Further, most inhibitory neurons' soma do not show spike frequency adaptation so excitatory-inhibitory (I-E) synapses would not show adaptation either. Thus the dendritic spike frequency adaptation mechanism is likely to influence the excitatory-excitatory (E-E) synapses. In this simple averaged neuron model, we have modeled this phenomenon by the adaptation of E-E synapses, which results in an effective decay of excitatory synapses with increasing duration in the up state. This does not rule out the contribution of other mechanisms to adaptation.

The central result of our paper is that for *nonuniform* networks composed of groups of excitatory and inhibitory neurons with strong coupling inside each group but weak coupling between groups, we encounter a *partial* synchronization transition associated with the onset of coherent UDS oscillations at very weak "long-range" synaptic coupling. Strong deterministic noise appears near the synchronization threshold due to *dephased* oscillatory activity of the individual networks. As the coupling strength increases, synchronization of *all* up-state activity does take place via a Kuramoto-type transition, but this requires making the long-range synaptic strength equal to the short-range synaptic strength. Up-state deterministic noise disappears in this limit.

The paper is organized as follows. In Sec. II we present the model. In Sec. III, we discuss the dynamics and phase diagram for the case of a uniform network of neurons. In Sec. IV we examine the properties of coupled groups of neurons and present the evidence for a synchronization transition combined with the appearance of deterministic noise in the up states.

II. POINT-NEURON MODEL WITH ADAPTATION

In this section we present the equations for a network of neurons in the presence of DSFA. Excitatory neurons will be represented by two dynamical variables: a "fast" membrane potential $v(t)$ of the soma of the neuron and a "slow" adaptation parameter $c(t)$ that measures the degree of adaptation of the dendrites of the excitatory neurons to prolonged input. In contrast, inhibitory neurons are represented only by a fast membrane potential with no adaptation variable. The DSFA process is described as follows. In the down-state part of the cycle, the adaptation level $c(t)$ is sufficiently high for excitatory neurons to be unable to stimulate other excitatory neurons. Neural activity dies down and only very weak, residual, firing

activity remains. The time scale for the down part of the cycle is determined by the *recovery time* of the adaptation process, which is taken to be in the range of seconds (e.g., the time scale required for pumping out excess Ca^{2+}). When $c(t)$ has been sufficiently reduced, excitatory neurons can start to activate each other, initiated by a low residual firing activity. Excitatory postsynaptic potentials (EPSPs) are generated as a result. Inhibitory neurons become active as well and start to generate inhibitory postsynaptic potentials (IPSPs), with the membrane potential $v(t)$ of both types of neurons remaining below threshold. The adaptation parameter now starts to rise due to EPSPs generated by excitatory neurons. This gradually suppresses the up-state positive feedback between excitatory neurons causing the up state to die down, after which the cycle starts again.

A. Model equations

We will separately discuss the rate equations obeyed by $v(t)$ and $c(t)$. The membrane potential $v_e^n(t)$ of the nth excitatory neuron of the network is assumed to obey—apart from the DSFA process—the conventional rate equation of the point neuron model:

$$\frac{dv_e^n}{dt} = -\frac{1}{\tau_e} v_e^n + \sum_m J_{ee}^{nm}(c^n) r^m\left(v_e^m\right) + \sum_k J_{ei}^{nk} r^k\left(v_i^k\right). \quad (2.1)$$

Inhibitory neurons obey a similar equation:

$$\frac{dv_i^n}{dt} = -\frac{1}{\tau_i} v_i^n + \sum_k J_{ii}^{nk} r^k\left(v_i^k\right) + \sum_m J_{ie}^{nm} r^m\left(v_e^m\right). \quad (2.2)$$

Note that there is no dependence on the adaptation variable in Eq. (2.2). The spiking rate tracks the time-averaged subthreshold membrane potential, as evidenced by a vast amount of literature. Thus $v_{e,i}^k$ is the time-averaged subthreshold potential of the kth excitatory (e) or inhibitory (i) neuron.

In these two equations, the first term on the right-hand side (RHS) represents the relaxation of the membrane potential to its equilibrium value. The membrane relaxation time constants τ_e and τ_i (with $\tau_e \sim 20$ ms for excitatory neurons and $\tau_i \sim 10$ ms for inhibitory neurons) are much shorter than the time scale of the up-down state oscillations. The resting potential will be assumed to be the same for all neuron types and all potentials will be measured with respect to the common resting potential. Positive and negative values for v thus correspond to depolarized and hyperpolarized membrane potentials, respectively. The second and third terms on the RHS represents the rate of change of the membrane potential due to EPSPs and IPSPs. The sums are over all neurons m that make a synaptic connection to neuron n. Here, r^n is the voltage-dependent firing rate of neuron n. Next, the strengths of synaptic connections from neuron m to neuron n are given by the matrix elements J^{nm} (superscripts will always refer to the neuron index). Positive (negative) entries correspond to excitatory (inhibitory) input. The subscripts ee, ii, ie, and ei of the matrix elements denote, respectively, synaptic connections from excitatory to excitatory neurons (J_{ee}, positive), from inhibitory to inhibitory neurons (J_{ii}, negative), from excitatory to inhibitory (J_{ie}, positive), and from inhibitory to excitatory junctions (J_{ei}, negative). Only the excitatory-excitatory synapses are assumed to be subject to DSFA so only $J_{ee}(c)$ depends on the adaptation parameter. For these excitatory-excitatory matrix entries, the synaptic strength will be assumed to rapidly decrease if the adaptation parameter c exceeds a threshold c^*. We will assume a sigmoidal dependence on c:

$$J_{ee}(c) = \frac{J_{ee}(0)}{1 + \exp[(c - c^*)/g_c]}. \quad (2.3)$$

The parameter g_c, the width of the transition region, can be varied to examine the dependence of up-down state dynamics on the sharpness of the onset of adaptation. In the numerical results discussed below, we took g_c equal to 3 and verified that our results were not qualitatively altered when we allowed g_c to vary. The parameter c^* is the value of the adaptation parameter where the synaptic strength has dropped by a factor of 2 from its maximum value $J_{ee}(0)$ (we used $c^* = 10$). Recall from our earlier discussion that one should expect c to oscillate around c^*. We will use the maximum synaptic strength $J_{ee}(0)$ as the central control parameter. It measures the maximum possible positive feedback between excitatory neurons. The particular functional form of Eq. (2.3) would follow from a two-state "open-closed" model [39] for adaptation but the precise form is not essential. Next, the dependence of the firing rate of a neuron on its membrane potential will be assumed to be of a standard form

$$r(v_{e,i}) = \frac{r_m}{1 + \exp[-(v_{e,i} - v^*)/g_{e,i}]}. \quad (2.4)$$

Here, r_m ($\sim$70 Hz) is the maximal firing rate in a completely depolarized state while v^* is the threshold firing potential. We find that $g_e > g_i$ (i.e., the firing rate dependence on the membrane potential is sharper for the inhibitory neurons than it is for the excitatory ones) is required to ensure the stability of the UDS oscillations within the model. This remains to be tested and constitutes a prediction necessary for the validity of our approach. The assumption is consistent with the common observation that inhibitory neurons typically have higher firing rates than excitatory neurons *in vivo*. For the numerical work presented here, we fix $g_e = 5$ mV for excitatory neurons and $g_i = 2$ mV for inhibitory neurons.

For the rate equation of the adaptation parameter for excitatory-excitatory synapses, we use a description similar to that of Fuhrmann *et al.* [36]:

$$\frac{dc^n}{dt} = -\frac{1}{\tau_c} c^n + \Delta c \sum_m r_e^m\left(v_e^m\right). \quad (2.5)$$

Here, c^m represents the mean adaptation level of the excitatory-excitatory synapses of excitatory neuron m. The adaptation recovery time τ_c will be taken to be 0.5 s. The sum on the RHS is over the excitatory neurons that make a synaptic junction with neuron n. The increase of the mean adaptation parameter Δc per incoming action potential will be a second important control parameter.

III. UNIFORM NETWORKS OF EXCITATORY AND INHIBITORY NEURONS

In this section we will examine the equations presented in Sec. II, first analytically and then numerically, for the case of two coupled, uniform networks. The first network is composed

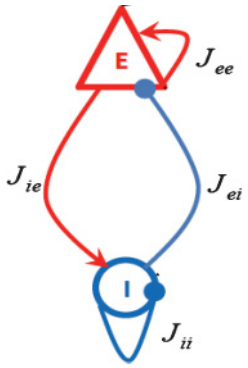

FIG. 3. (Color online) Coupled groups of excitatory (E) and inhibitory (I) neurons. Excitatory synaptic connections are indicated by arrows (J_{ee} from excitatory to excitatory neurons and J_{ie} from excitatory to inhibitory neurons). Inhibitory connections are shown as lines ending in a dot (J_{ii} from inhibitory to inhibitory neurons and J_{ei} from inhibitory to excitatory neurons).

of identical excitatory neurons, all with the same connectivity, and the second network is composed of identical inhibitory neurons, again with the same connectivity. Recall here that the competition between excitatory and inhibitory neurons is an essential feature of UDS oscillations. The two groups of neurons are connected together as shown in Fig. 3.

There are three dynamical variables: the common membrane potential $v_e(t)$ of the group of identical excitatory neurons, the common membrane potential $v_i(t)$ of the group of identical inhibitory neurons, and the adaptation parameter $c(t)$ of the excitatory-excitatory synapses. The three corresponding rate equations are

$$\frac{dv_e}{dt} = -\frac{1}{\tau_e}v_e + N_e J_{ee}(c) r(v_e) + N_i J_{ei} r(v_i), \tag{3.1}$$

$$\frac{dv_i}{dt} = -\frac{1}{\tau_i}v_i + N_i J_{ii} r(v_i) + N_e J_{ie} r(v_e), \tag{3.2}$$

$$\frac{dc}{dt} = -\frac{1}{\tau_c}c + N_e \Delta c\, r(v_e). \tag{3.3}$$

Here, N_e is the number of excitatory neurons of the network times the probability that they are connected to one particular neuron. A similar definition applies to N_i. Because the adaptation parameter varies on a significantly longer time scale than the two potentials, we start by assuming separation of time scales, and examine Eqs. (3.1) and (3.2) as a pair of dynamical equations, treating c as a parameter.

A. Down-state fixed point

In the down state, membrane potentials are significantly below the firing threshold. Exploiting the fact that the firing onset is quite sharp for the inhibitory neurons, we will neglect firing by inhibitory neurons in the down state and set $r(v_i)$ to zero. For a given value of the adaptation parameter, we are then left with just a single equation for the excitatory potential:

$$\frac{dv_e}{dt} \approx -\frac{1}{\tau_e}v_e + N_e J_{ee}(c) r(v_e). \tag{3.4}$$

The inhibitory potential is determined by the excitatory potential through

$$\frac{dv_i}{dt} \approx -\frac{1}{\tau_i}v_i + N_e J_{ie} r(v_e). \tag{3.5}$$

In the hyperpolarized down state, where the potential is very close to the resting potential [which is zero in the absence of excitatory input—see Eq. (3.4)], we will assume $|v_e/g_e| \ll 1$. We can then expand the firing rate for excitatory neurons Eq. (2.4) in a Taylor series in powers of v_e/g_e,

$$r(v_e) \approx r_m \exp(-v^*/g_e)\left[1 + (v_e/g_e) + \tfrac{1}{2}(v_e/g_e)^2 + \cdots\right] \tag{3.6}$$

since the saddle-node bifurcation occurs at small v_e, as can be verified *post hoc* in Fig. 5; we also used $\exp(-v^*/g_e) \ll 1$ to neglect terms of order $\exp(-2v^*/g_e)$. If one inserts Eq. (3.6) into Eq. (3.4), one recovers an equation of the form

$$\frac{dx}{dt} \approx A + Bx + Cx^2. \tag{3.7}$$

Here, $B = -\frac{1}{\tau_e} + N_e(r_m/g_e)J_{ee}(c)\exp(-v^*/g_e)$ can have either sign while $A = N_e J_{ee}(c) r_m \exp(-v^*/g_e)$ and $C = \frac{1}{2}N_e(r_m/g_e^2)J_{ee}(c)\exp(-v^*/g_e)$ are both positive. Note that the effect of a given synaptic strength $J_{ee}(c)$ on the system's dynamics is exponentially reduced by the factor $\exp(-v^*/g_e)$. Equation (3.7) is a classical illustration of a one-dimensional saddle-node bifurcation. Fixed points of Eq. (3.7) are found by setting the RHS of Eq. (3.7) to zero so $dx/dt = 0$. There are either two real solutions $x_\pm = \frac{-B \pm \sqrt{B^2 - 4AC}}{2}$ for $B^2 - 4AC$ positive, one stable and one unstable, or there are none. For positive B, the two fixed points are hyperpolarized (negative v). For negative B, these fixed points are weakly depolarized (positive v). In the v_e-v_i diagram of Fig. 4, the approaching bifurcation is shown schematically as a node with a nearby saddle point, both located on the $\frac{dv_i}{dt} = 0$ null cline, which is parabolic—see Eq. (3.6)—and independent of c.

Using the earlier expressions for A, B, and C, it follows that $B^2 - 4AC$ equals $(\frac{1}{\tau_e})^2 - \frac{2}{\tau_e}N_e(r_m/g_e)J_{ee}(c)\exp(-v^*/g_e)$. If

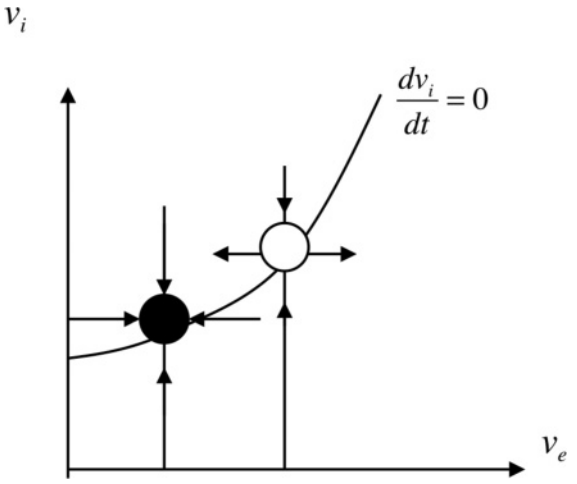

FIG. 4. Stable node and unstable saddle fixed points characterizing the down state. The curve denoted by $\frac{dv_i}{dt} = 0$ is the null cline $\frac{1}{\tau_i}v_i = N_e J_{ie} r(v_e)$.

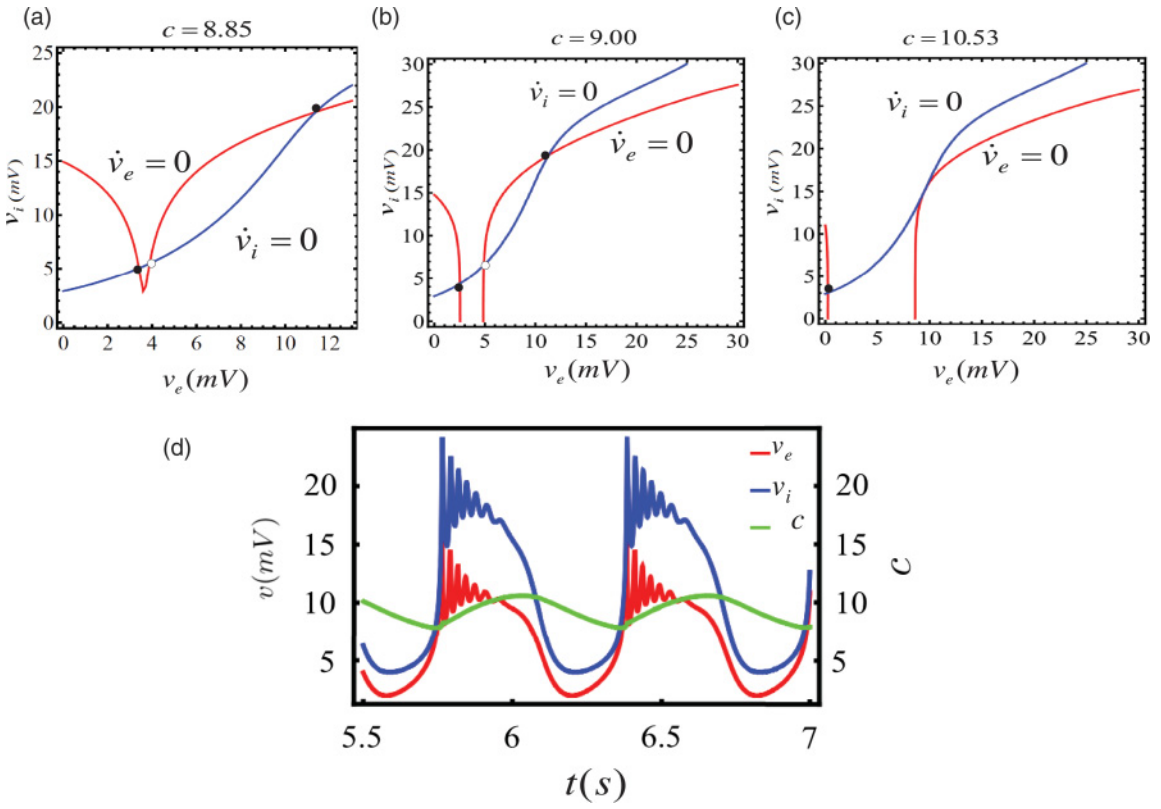

FIG. 5. (Color online) (a) Null clines of the excitatory and inhibitory potentials during an up state (upper solid circle). The up state is characterized by a stable spiral fixed point. A down-state saddle-node pair (solid and open circle) has just appeared by a saddle-node bifurcation so the system is bistable. (b) As the adaptation parameter c continues to increase, the saddle begins to move rightward along the $\dot{v}_i = 0$ null cline and will eventually annihilate the up-state fixed point. (c) Null clines at the saddle-node bifurcation that destabilized the up state. (d) Up-down states of the uniform network model. Parameters were tuned so (i) the up-state potential remains somewhat below the firing threshold of 30 mV and (ii) the decay time of the up-state weakly overdamped oscillation is long compared to the period. The system is close to a Hopf bifurcation where the up-state activity would turn into a limit cycle.

$J_{ee}(c)$ is increased, $B^2 - 4AC$ decreases and the two fixed points merge when the synaptic strength reaches a critical value

$$J^* \sim \frac{g_e}{2N_e\tau_e r_m}\exp(v^*/g_e). \tag{3.8}$$

For $J_{ee}(c)$ larger than J^* there are no fixed points associated with the down state. Both inhibitory and excitatory potentials then flow to an up-state fixed point close to the firing threshold, as discussed below.

B. Up-state fixed point

Start from an initial state where there are no down-state fixed points (so $B^2 < 4AC$). The rate equations cause the system to flow to the up-state fixed point. In that regime, the adaptation parameter is (slowly) increasing. This leads to a slow decrease of $J_{ee}(c)$ and thus of B. Eventually B falls below $-2\sqrt{AC}$ and the down-state saddle-node pair reappears. This does *not* terminate the up state, however. The mathematical analysis of the up-state fixed point is more involved than that of the down-state fixed point and is give in the Appendix. Here, we will illustrate the results combining numerical solution with simple arguments.

Figure 5(a) shows the numerically obtained null clines $\frac{dv_i}{dt} = 0$ and $\frac{dv_e}{dt} = 0$ for a value of c in the v_e-v_i diagram where the down-state saddle-node pair has just reappeared (analytic expressions for the null clines are given in the Appendix).

In Figs. 5(a) and 5(b), the up-state fixed point is shown as the top intersection of the two null clines, somewhat below the firing threshold at 30 mV. A pair of down-state fixed points has just appeared at the lower left-hand corner in Fig. 5(a). The evolution of those fixed points with increasing c is shown in Fig. 5(b). In the Appendix the membrane potentials of the up-state fixed point are shown to be

$$v_i^* - v^* \approx -g_i \ln[\tau_i r_m N_i J_{ie}|J_{ei}|/J_{ee}(c)g_i], \tag{3.9a}$$
$$v_e^* - v^* \approx -g_e \ln(\tau_i r_m N_e J_{ie}/g_i). \tag{3.9b}$$

Note that Eq. (3.9a) but not (3.9b) depends on the adaptation parameter. Equation (3.10) shows for what combination of synaptic strengths the operating point of the network are set somewhat below the firing threshold v^*: The dimensionless parameters $\Gamma_i \equiv [\tau_i r_m N_i J_{ie}|J_{ei}|/J_{ee}(c)g_i]$ and $\Gamma_e \equiv (\tau_i r_m N_e J_{ie}/g_i)$ both have to exceed one. In that case the fixed-point potentials are located roughly within a distance $g_{i,e}$ of the firing threshold.

This last result is important. Because the logarithmic function is only weakly dependent on its argument, locating

the fixed point somewhat below the firing threshold is quite "robust:" The fixed point hardly shifts if the synaptic strengths are changed as long as the two parameters exceed one. *Individual* neurons do not have a "natural" setting for the membrane potential to be pegged a bit below the firing threshold. The stability of this setting is produced here by the interplay between the excitatory and inhibitory neurons. Note that by allowing these parameters to drop below one, it also is possible to significantly "turn up" the firing rate, as might happen during awakening.

In a linear stability analysis of this fixed point (v_e^*, v_i^*), small deviations around the new fixed point are described by

$$\begin{pmatrix} \delta\dot{v}_e \\ \delta\dot{v}_i \end{pmatrix} = \begin{pmatrix} a_{11} & a_{12} \\ a_{21} & a_{22} \end{pmatrix} \begin{pmatrix} \delta v_e \\ \delta v_i \end{pmatrix}. \tag{3.10}$$

Here, $a_{11} = -\frac{1}{\tau_e} + N_e J_{ee}(c) r'(v_e^*)$, $a_{12} = N_i J_{ei} r'(v_i^*)$, $a_{21} = N_e J_{ie} r'(v_e^*)$, and $a_{22} = -\frac{1}{\tau_i} + N_i J_{ii} r'(v_i^*)$. The eigenvalues $\lambda_{1,2} = \frac{\mathrm{Tr} \pm \sqrt{\mathrm{Tr}^2 - 4\Delta}}{2}$, with $\mathrm{Tr} = a_{11} + a_{22}$ the trace and $\Delta = a_{11}a_{22} - a_{12}a_{21}$ the determinant, determine the fate of small deviations of the fixed point. The slope of the $\frac{dv_i}{dt} = 0$ null cline must exceed the slope of the $\frac{dv_e}{dt} = 0$ null cline at the fixed point in order for there to be an intersection [see Fig. 5(a)]. The equation for the $\frac{dv_i}{dt} = 0$ null cline is, according to Eq. (3.10), $a_{11}\delta v_e + a_{12}\delta v_i = 0$, and that of the $\frac{dv_e}{dt} = 0$ null cline $a_{21}\delta v_e + a_{22}\delta v_i = 0$. The $\frac{dv_i}{dt} = 0$ null cline has the largest slope if $(-\frac{a_{11}}{a_{12}})$ is less than $(-\frac{a_{21}}{a_{22}})$. According to this last condition, the sign of the determinant $\Delta = a_{11}a_{22} - a_{12}a_{21}$ has to be positive, keeping in mind that both a_{11}/a_{12} and a_{21}/a_{22} are negative. This means that the eigenvalues either are both real with the same sign—in which case the fixed point is again a node—or that they are complex conjugates, in which case the trajectories must spiral either in or out. Drawing the flow vectors in Fig. 5(b) produces spiral trajectories corresponding to overdamped oscillations. The eigenvalues are complex conjugates, which means that $\mathrm{Tr}^2 - 4\Delta$ must be negative. The imaginary part $\Omega = \frac{1}{2}\sqrt{4\Delta - \mathrm{Tr}^2}$ of the eigenvalue is the frequency scale of the oscillations in the up state. For negative values of the trace, the real part of the eigenvalues is negative and the up-state fixed point corresponds to a stable spiral. The flow lines spiral inward to the fixed point with a characteristic time scale equal to $-2/\mathrm{Tr}$. For positive values of the trace, the flow lines spiral outward and approach a limit cycle: The point $\mathrm{Tr} = 0$ marks a Hopf bifurcation. The "critical regime," with Tr small compared to the oscillation frequency Ω, is the appropriate operating point for the start of the up-state period, in a theory of up-state activity with persistent oscillatory activity due to competition between inhibitory and excitatory neurons.

In the Appendix, the matrix elements are shown to be given approximately by

$$a_{11} \approx -\frac{1}{\tau_e} + \frac{1}{\tau_i}\left(\frac{g_i}{g_e}\right)\frac{J_{ee}(c)}{J_{ie}}, \tag{3.11}$$

$$a_{12} \approx -\frac{1}{\tau_i}\frac{J_{ee}(c)}{J_{ie}}, \tag{3.12}$$

$$a_{22} \approx -\frac{1}{\tau_i} - \frac{1}{\tau_i}\frac{|J_{ii}|J_{ee}(c)}{J_{ie}|J_{ei}|}, \tag{3.13}$$

$$a_{21} \approx \frac{1}{\tau_i}. \tag{3.14}$$

The decay rate of the oscillation is given by

$$-\mathrm{Tr} \approx \frac{1}{\tau_e} + \frac{1}{\tau_i} - \frac{1}{\tau_i}\frac{J_{ee}(c)}{J_{ie}}\left[\left(\frac{g_i}{g_e}\right) - \frac{|J_{ii}|}{|J_{ei}|}\right]. \tag{3.15}$$

Setting the trace to zero is possible only if the inhibitory-inhibitory synaptic coupling is sufficiently weak compared to the coupling between inhibitory and excitatory neurons, i.e., if $\frac{|J_{ii}|}{|J_{ei}|} < (\frac{g_i}{g_e})$. Assuming that this is the case, the condition of vanishing trace is

$$\frac{J_{ee}(c)}{J_{ie}} \approx \left(\frac{\tau_i}{\tau_e} + 1\right) \Big/ \left[\left(\frac{g_i}{g_e}\right) - \frac{|J_{ii}|}{|J_{ei}|}\right]. \tag{3.16}$$

If this condition is not quite obeyed, then the decay rate of the oscillation is equal to the trace. Note that increasing the adaptation parameter increases the decay rate of the oscillation, an effect visible in Fig. 5(c). Assuming that the trace has been set to zero, the resulting oscillation frequency $\Omega \approx \sqrt{(a_{11}a_{22} - a_{12}a_{21})}$ is

$$\Omega \approx \frac{1}{\tau_i}\sqrt{\left[\frac{\tau_i}{\tau_e} - \left(\frac{g_i}{g_e}\right)\frac{J_{ee}(c)}{J_{ie}}\right]\left(1 + \frac{|J_{ii}|J_{ee}(c)}{J_{ie}|J_{ei}|}\right) + \left(\frac{J_{ee}(c)}{J_{ie}}\right)\left(\frac{g_i}{g_e}\right)}. \tag{3.17}$$

A particular simple case occurs when one can neglect inhibitory-inhibitory coupling (i.e., $J_{ii} = 0$). In that case we find that the oscillation frequency

$$\Omega \approx \frac{1}{\sqrt{\tau_e \tau_i}} \tag{3.18}$$

is set by the *geometrical mean* of the excitatory and inhibitory membrane relaxation times, which is in the range of 10–100 Hz. The full solution with corrections due to the small, but nonzero, J_{ii} is shown in the Appendix. Examining that solution, we note that the oscillation frequency is generically larger than the geometric mean [Eq. (3.18)], but decreases toward that value near the termination of the up state.

We now consider the termination of the up state in more detail. An increase in the adaptation parameter c causes $J_{ee}(c)$ to decrease and the oscillation frequency to decrease. This is shown most simply by noting that the magnitude of the trace increases and must be included in the oscillation frequency since $\Omega = \frac{1}{2}\sqrt{4\Delta - \mathrm{Tr}^2}$. The spiral fixed point turns into a stable node when $\mathrm{Tr}^2 = 4\Delta$, at which point the eigenvalues of the matrix become real and oscillations stop. At the same time, the unstable fixed point moves up along the null cline $\frac{dv_i}{dt} = 0$,

as discussed above in Fig. 4. As discussed in the Appendix, the unstable fixed point is marked by a logarithmic singularity of the null cline.

The unstable fixed point fuses with the up-state fixed point when the two null clines share a common tangent, which is the case when $\Delta = 0$. This marks a new bifurcation where the up-state fixed point disappears. Figure 5(c) shows an example where the stable and unstable fixed points have just fused through a saddle-node bifurcation. In the Appendix we show that this bifurcation is determined by the condition that $J_{ee}(c)$ drops below a threshold $J^*_{ee} \equiv (g_e\tau_i/g_i\tau_e)J_{ie}$. For values of $J_{ee}(c)$ below J^*_{ee}, the flow lines drive the system back to the stable down-state fixed point, after which the cycle starts again.

A picture emerges of a sequence of up-down state oscillations as a periodic cycle where an unstable fixed point shuttles up and down the $\frac{dv_i}{dt} = 0$ null cline, alternatingly destroying the down-state and the up-state stable fixed points through a series of repeated saddle-node bifurcations. In order to verify this analysis, we carried out a numerical analysis of the full set of equations. Figure 5(c) shows two successive periods, computed numerically. The coexistence of the two stable fixed points separated by an unstable fixed point, shown by the first arrow, corresponds to Fig. 5(a). The unstable fixed point slides up the null cline and, at the point indicated by the second arrow, at the end of the up cycle, it annihilates the stable fixed point of the up state, corresponding to Fig. 5(b), consistent with our analysis. For the choice of parameters for Fig. 5(c), the up-state oscillations clearly are weakly underdamped with $|\mathrm{Tr}| \ll \Omega$: The system is close to a Hopf bifurcation. The excitatory and inhibitory oscillations track each other while the adaptation parameter slowly oscillates around the set point c^*=10.

The sequence of up-down states of Fig. 5(c) appears to be strictly periodic, but this is not the case. If one tracks the trajectory over many successive cycles in the v_i-v_e plane, computed numerically, then an irregular precession of oscillatory orbits is encountered, shown in Fig. 6(a).

This irregular precession is in fact visible in a plot of the firing rate, as shown in Fig. 6(b). The fact that the orbits

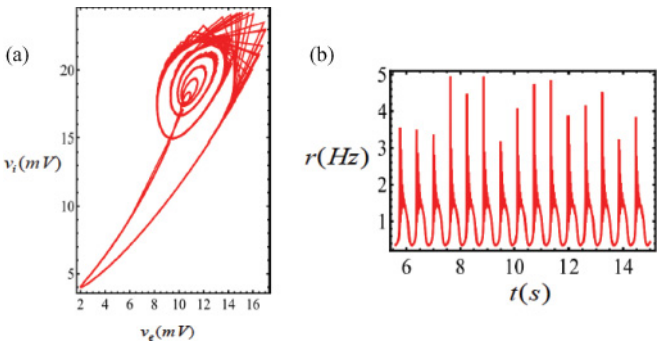

FIG. 6. (Color online) (a) Trajectory of the excitatory and inhibitory potentials for the same parameters as Fig. 5 but now for many periods. The up-state activity shows as a spiral trajectory ending at the up-state fixed point at the upper right-hand corner. The failure of the up-state orbits to close means that the system cannot be described perfectly as two dimensional (see text). The down-state fixed point is at the lower left-hand corner. (b) The precession of the potential maxima is visible in the firing rate, which is dominated by the maxima of the potential.

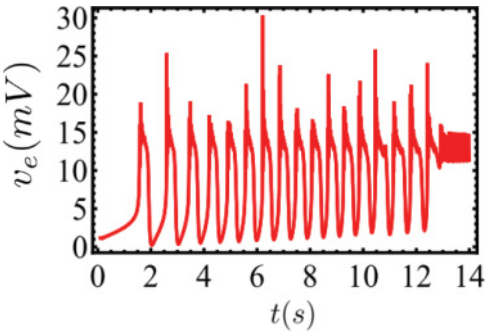

FIG. 7. (Color online) Membrane potential as a function of time if the excitatory synaptic strength slowly increases.

in the v_e-v_i fail to close exactly must mean, according to the Poincaré-Bendixson theorem [1], that, notwithstanding the difference in time scales between the adaptation parameter and the rapid up-state oscillations, the dynamics cannot be described by only two coupled equations. However, Fig. 5(c) demonstrates that these effects are difficult to see in a recording of the membrane potential.

One could speculate that this model for up-down state oscillations could be used as a simple description for the gradual awakening from deep sleep (or anesthesia) by a slow increase of the positive feedback between excitatory neurons, i.e., by increasing the synaptic strength $J_{ee}(0)$ linking excitatory neurons. We assume that $J_{ee}(0)$ slowly increases as animals become more awake. This could be mediated by a variety of cellular mechanisms. For example, neuromodulators change neural excitability as well as short-term plasticity. The neuromodulator concentrations change with behavioral state and thus can alter the strength of neural connectivity. This modulation can influence differentially the excitatory and inhibitory neurons. For instance, acetylcholine alters the excitatory neurons' spike frequency adaptation and cholinergic levels change with the sleep-wake cycle. Dopamine has a distinct effect on excitatory and inhibitory inputs. As shown in Fig. 7, the model predicts that the UDS period shortens when $J_{ee}(0)$ increases, while the fraction of time spent in the down state goes to zero.

There is a point where the down state completely disappears, leaving the system permanently in the up state, still with rapid oscillations due to the feedback between excitatory and inhibitory neurons. These are in fact features that have been reported in studies of awakening and, in a future publication, we will compare theory and experiment.

An important problem with the uniform network description of this section is that the computed activity of the up-state potential is much more regular than the measured noisy up-state activity displayed in Fig. 1. In fact, there is little resemblance between Figs. 1 and 5(c). In the next section, we will show that network geometry plays a crucial role in terms of up-state activity.

IV. SYNCHRONIZATION TRANSITION

In this section we will examine the model for the simplest case of a *nonuniform* network: two weakly coupled network pairs, each of the form discussed in Sec. II. The two coupled network pairs (1 and 2) are shown in Fig. 8.

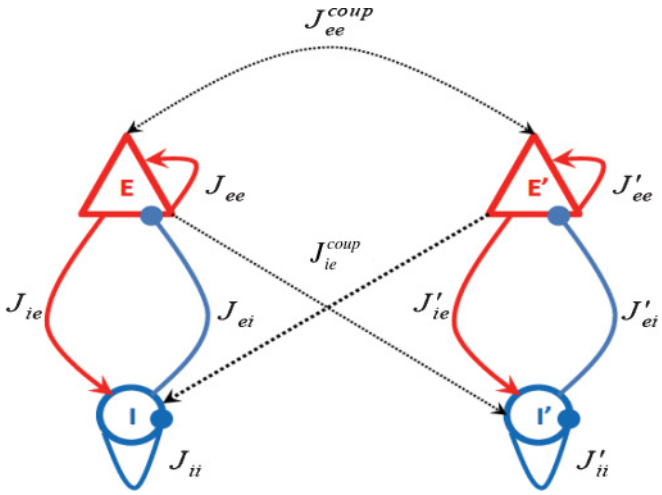

FIG. 8. (Color online) Two weakly coupled, uniform networks of excitatory and inhibitory neurons.

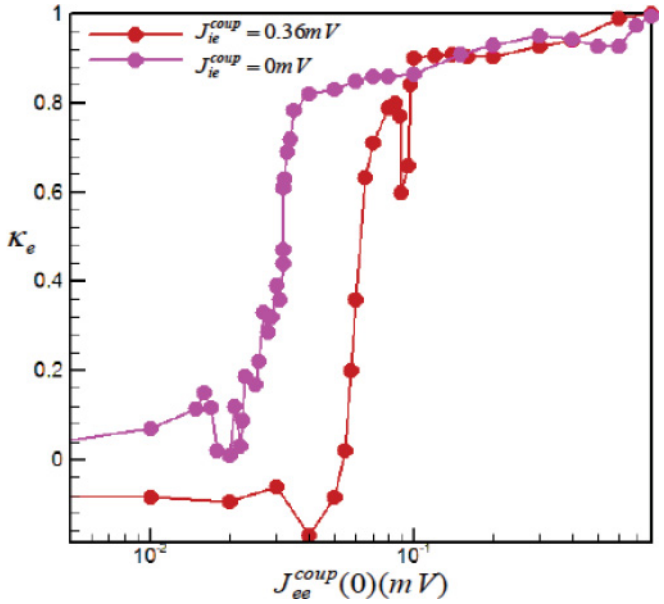

FIG. 9. (Color online) Correlation coefficient κ_ε for the excitatory potential of two networks of Fig. 8 as a function of the long-range excitatory-excitatory synaptic strength $J_{ee}^{\rm coup}(0)$ for two different values of the long-range excitatory-inhibitory synaptic strength $J_{ie}^{\rm coup}$. A partial synchronization transition takes place when $J_{ee}^{\rm coup}(0)$ is of the order of 10^{-2} mV, about two orders of magnitude less than the short-range synaptic strengths (about 1 mV). Full synchronization requires an increase of $J_{ee}^{\rm coup}(0)$ to about 1 mV.

The synaptic strengths of network 2 are indicated by primes. The two network pairs are assumed to have the same number of excitatory and inhibitory neurons. Note that only "long-range" excitatory-excitatory and excitatory-inhibitory connections are included: All excitatory neurons of network pair 1 are coupled to all excitatory neurons of network pair 2 with the same "long-range" synaptic strength $J_{ee}^{\rm coup}$ and to all inhibitory neurons of network 2 by the synaptic strength $J_{ie}^{\rm coup}$ (and vice versa). The two coupled network pairs are described by six rate equations:

$$\frac{dv_e}{dt} = -\frac{1}{\tau_e}v_e + N_e J_{ee}(c)r(v_e) + N_i J_{ei} r(v_i) + N_e J_{ee}^{\rm coup}(c)r(v'_e), \tag{4.1}$$

$$\frac{dv_i}{dt} = -\frac{1}{\tau_i}v_i + N_i J_{ii} r(v_i) + N_e J_{ie} r(v_e) + N_e J_{ie}^{\rm coup} r(v'_e), \tag{4.2}$$

$$\frac{dc}{dt} = -\frac{1}{\tau_c}c + N_e \Delta c\, r(v_e) + N_e \Delta c\, r(v'_e), \tag{4.3}$$

$$\frac{dv'_e}{dt} = -\frac{1}{\tau_e}v'_e + N_e J'_{ee}(c')r(v'_e) + N_i J'_{ei} r(v'_i) + N_e J_{ee}^{\rm coup}(c')r(v_e), \tag{4.4}$$

$$\frac{dv'_i}{dt} = -\frac{1}{\tau_i}v'_i + N_i J'_{ii} r(v'_i) + N_e J'_{ie} r(v'_e) + N_e J_{ie}^{\rm coup} r(v_e), \tag{4.5}$$

$$\frac{dc'}{dt} = -\frac{1}{\tau_c}c' + N_e \Delta c\, r(v'_e) + N_e \Delta c\, r(v_e). \tag{4.6}$$

The long-range excitatory-excitatory connections $J_{ee}^{\rm coup}(c)$ depend on the adaptation parameter again according to Eq. (2.3). In order to characterize the degree of synchronicity between these two networks, we introduce a correlation coefficient

$$\kappa^{ij} = \frac{\langle v^i v^j\rangle - \langle v^i\rangle\langle v^j\rangle}{\sqrt{(\langle v^{i2}\rangle - \langle v^i\rangle^2)(\langle v^{j2}\rangle - \langle v^j\rangle^2)}} \tag{4.7}$$

for the membrane potentials of neuron i and j. The correlation coefficient is equal to zero if $v^i(t)$ is completely uncorrelated with $v^j(t)$ and one if the two are fully correlated [e.g., if $v^i(t)$ is proportional to $v^j(t)$]. Figure 9 shows the correlation coefficient between the potentials of excitatory neurons in the two networks as a function of the long-range synaptic strength $J_{ee}^{\rm coup}(0)$ for two different values of $J_{ie}^{\rm coup}$.

An abrupt synchronicity transition takes place for values of the long-range synaptic strength $J_{ee}^{\rm coup}(0)$ that are nearly two orders of magnitude less than the short-range synaptic strength $J_{ee}^{\rm coup}(0)$. As could be expected, the critical value of $J_{ee}^{\rm coup}(0)$ is lowest if the inhibitory coupling $J_{ie}^{\rm coup}$ between the two networks is zero. If $J_{ie}^{\rm coup} = 0$ and if $J_{ee}^{\rm coup}(0)$ is less than 0.02 mV, then correlation is negligible. Between 0.03 and 0.04 mV, the correlation coefficient rises to about 0.8. A further increase of the correlation coefficient to (nearly) 1 requires a further increase of $J_{ee}^{\rm coup}(0)$ to about 1 mV, comparable to the "short-range" excitatory synaptic strength in the up state, so an increase by more than a decade. Relatively large values of $J_{ie}^{\rm coup}$ do not change these observations, except for a mild increase of the synchronization threshold and a (puzzling) sharp drop in correlation just beyond the threshold.

Figure 10 shows three periods of the coupled networks for $J_{ee}^{\rm coup}(0)$ values just beyond the sharp increase of the correlation coefficient. The up-down state sequence of the two network pairs are indeed locked together. In particular, the onset times of the up states are nearly exactly the same. This is not true for the *termination* of the up states: For the second and third cycles, network 2 remains in the up state after network 1 has switched to the down state. The minima of the potentials in the respective

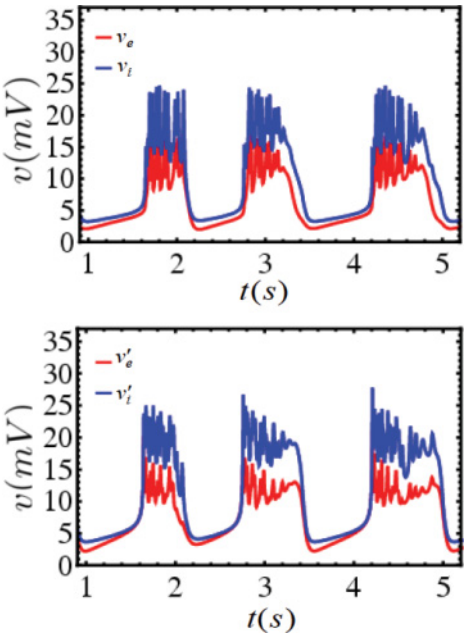

FIG. 10. (Color online) Excitatory and inhibitory potential of the two coupled networks close to the synchronization transition. The onset of the up state is synchronized but the decay of the up state is not. The period of the oscillations and the duration of the down state show significant statistical variation. The up-state activity is stochastic, with little correlation between the two networks.

down states are again synchronized, however. *Synchronization is thus established in the down-state part of the cycle*. Next, note that the durations of the up and down states are variable, as is the case for actual UDS oscillations (see Fig. 1). Finally, the up-state potential variations no longer perform the weakly underdamped harmonic oscillations of Sec. III, but instead appear to be highly stochastic, with pronounced differences between different cycles, another feature consistent with Fig. 1. Up-state activity during the first period has the character of a noisy limit cycle. During the second and third period, an initial limit cycle appears to change to weakly underdamped noisy oscillation. The inhibitory and excitatory potentials within each of the two networks remain correlated, but for the high-frequency up-state activity there appears to be little or no correlation between the two networks. The 20% reduction of the network-network correlation coefficient below its maximum value after the synchronization transition is a combination of this incoherence plus the differences in the decay times of the up states noted earlier.

We can analyze the partial synchronization transition and specifically the effect coupling two UDS oscillators has on suppressing the coherent ringing in the up state by examining the power spectrum of $v_e(t)$. We first do this for a single UDS oscillator and then for two UDS oscillators, coupled so that they are partially synchronized, as discussed above. In Fig. 11 we plot first a representative trace of the excitatory neurons' membrane potential and then the power spectrum (amplitude versus frequency) of that signal measured at 1000 Hz in overlapping 1-s time windows, using a Hamming filter to suppress the amplitude leakage into the side lobes [40]. The amplitude (in arbitrary units) is shown by a color (grayscale)

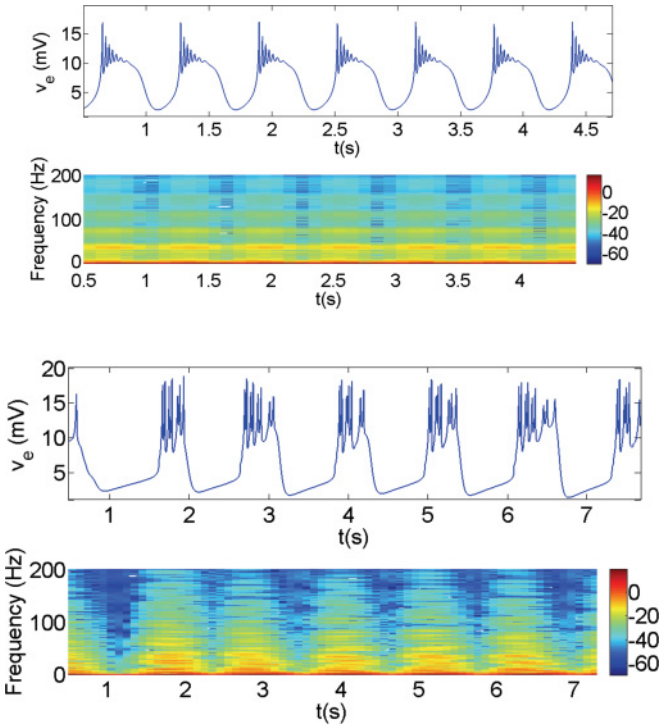

FIG. 11. (Color online) The upper panel shows a representative trace of the membrane potential of the excitatory neurons in a single UDS ocscillator and the power spectral density of the signal measured in a one second window—see text for details. The up states of the single UDS oscillator show a peak in the power spectrum around 75 Hz, consistent with our analysis. See Eq. (3.18). In the lower panel, this peak is lost in the coupled UDS oscillator system, which shows a broad power spectrum in the up states.

code, with the "hotter" colors representing higher amplitudes. The upper panel corresponds to a single UDS oscillator and shows pronounced ringing at a frequency predicted by Eq. (3.18). The lower panel, showing the analogous data for two coupled UDS oscillators shows that, due to partial synchronization, the up-state signal now has broad frequency content, demonstrating the suppression of that ringing. The up and down states of the two oscillators, however, remain in phase. Comparing the observed frequency content of the up state in the coupled UDS oscillator model in the partial synchronization regime to experimental data may prove to be a useful way to further constrain model parameters.

The large difference between the values of $J_{ee}^{\mathrm{coup}}(0)$ required for up-down synchronization as compared to complete synchronization can be understood by a simple fixed-point analysis. Assume first that both systems are located at the down-state stable fixed point, with similar values for the adaptation parameter. Then assume that network 2 *but not network 1* passes through a saddle-node bifurcation, destabilizing the down-state fixed point. The excitatory potential of network 1 then obeys

$$\frac{dv_e}{dt} \approx -\frac{1}{\tau_e}v_e + N_e J_{ee}(c) r(v_e) + N_e J_{ee}^{\mathrm{coup}}(c)\langle r(v'_e)\rangle. \quad (4.8)$$

Here, $\langle r(v'_e)\rangle$ is the average up-state firing rate of network pair 2 (about 5 Hz, say). Expanding again in powers of v_e, we

recover the earlier saddle-node bifurcation equation $\frac{dx}{dt} \approx A + Bx + Cx^2$ with B and C the same value as before. However,

$$A = N_e J_{ee}(c)[r_b + r_m \exp(-v^*/g_e)] + N_e J_{ee}^{\text{coup}}(c)\langle r(v_e')\rangle. \tag{4.9}$$

In order for the long-range network-network coupling to trigger a *second* saddle-node bifurcation in network pair 1, a critical long-range coupling constant is needed of

$$J_{ee}^{\text{coup}}(0)^* = J_{ee}(0)\left[\frac{r_m \exp(-v^*/g_e)}{r(v_e')}\right]. \tag{4.10}$$

The factor in brackets is just the ratio between the firing rates in the up and in the down states, about 10^{-2} for our estimates. It is immediately clear that very weak long-range interactions suffice to synchronize the saddle-node bifurcations of the UDS oscillations.

Turning to the termination of the up state, assume that the two networks both are in the up state with no coherence between the up-state oscillations (see below). For network 1, we average over the up-state activity of network 2 (and vice versa) so

$$\frac{dv_e}{dt} = -\frac{1}{\tau_e}v_e + N_e J_{ee}(c) r(v_e) + N_i J_{ei} r(v_i) + N_e J_{ee}^{\text{coup}}(c)\langle r(v_e')\rangle_2, \tag{4.11}$$

$$\frac{dv_i}{dt} = -\frac{1}{\tau_i}v_i + N_i J_{ii} r(v_i) + N_e J_{ie} r(v_e) + N_e J_{ie}^{\text{coup}}\langle r(v_e')\rangle_2. \tag{4.12}$$

If network 2 undergoes the up-state saddle-node bifurcation, and stops firing, then the last terms of the two equations are removed. Will this again trigger a second saddle-node bifurcation in network 1? The term $N_e J_{ee}^{\text{coup}}(c)\langle r(v_e')\rangle_2$ does increase the separation of the excitatory potential saddle-node pair and its suppression could trigger the second bifurcation. However, it is clear from Eq. (4.11) that this shift is significant only if $J_{ee}^{\text{coup}}(c)$ is roughly comparable in magnitude to $J_{ee}(c)$. It is thus clear why the up-down states are synchronized at the start of the up state by weak network-network coupling but *not* at the end of the up states.

Is this consistent with uncorrelated deterministic noise in the up state? Extending the linear stability analysis of Sec. III to the two coupled networks gives

$$\begin{pmatrix} \delta\dot{v}_e \\ \delta\dot{v}_i \\ \delta\dot{v}_e' \\ \delta\dot{v}_i' \end{pmatrix} = \begin{pmatrix} a_{11} & a_{12} & a_{13} & 0 \\ a_{21} & a_{22} & a_{23} & 0 \\ a_{31} & 0 & a_{11}' & a_{12}' \\ a_{32} & 0 & a_{21}' & a_{22}' \end{pmatrix} \begin{pmatrix} \delta v_e \\ \delta v_i \\ \delta v_e' \\ \delta v_i' \end{pmatrix}, \tag{4.13}$$

where we retained the earlier notation of the unperturbed 2×2 matrices for the unperturbed matrix elements of the 4×4 matrix. The new matrix elements coupling the networks are $a_{13} \approx a_{31} \approx N_e J_{ee}^{\text{coup}}(c)\frac{r_m}{g_e}$ and $a_{23} \approx a_{32} \approx N_e J_{ei}^{\text{coup}}\frac{r_m}{g_e}$. We will examine the effects of weak coupling between the two networks perturbatively in terms of a small parameter $\varepsilon = a_{13} = a_{23} = a_{31} = a_{32}$ (for simplicity, we equated the long-range coupling parameters). For $\varepsilon = 0$, the vectors $\vec{r}_1(t) = (\delta v_e, \delta v_i)$ and $\vec{r}_2(t) = (\delta v_e', \delta v_i')$ perform, as before, oscillations with frequencies $\Omega_{1,2} = \frac{1}{2}\sqrt{4\Delta_{1,2} - \text{Tr}_{1,2}^2}$ and damping rates $\text{Tr}_{1,2}$. Both oscillations are, by assumption, very weakly damped with $\Delta_{1,2} \gg \text{Tr}_{1,2}$. The frequency difference $(\Omega_1 - \Omega_2)$ between the two networks is assumed to be of the order of the frequencies themselves. Δ and Tr refer here to the determinant and trace of the matrices $\overleftrightarrow{M}_1 = \begin{pmatrix} a_{11} & a_{12} \\ a_{21} & a_{22} \end{pmatrix}$ and $\overleftrightarrow{M}_2 = \begin{pmatrix} a_{11}' & a_{12}' \\ a_{21}' & a_{22}' \end{pmatrix}$. We will look for solutions of Eq. (4.13) of the form $\vec{r}_{1,2}(t) = \vec{A}_{1,2}\exp i\varphi_{1,2}(t)$. Here, $\vec{A}_{1,2}$ are normalized eigenvectors of the two matrices $\overleftrightarrow{M}_{1,2}$ with eigenvalues $\lambda_{1,2}$. After inserting this expression into Eq. (4.13), one finds that the phase difference $\chi = \text{Re}(\varphi_1 - \varphi_2)$ between the two networks obeys

$$\frac{d\chi}{dt} \approx (\Omega_1 - \Omega_2) + \varepsilon\Delta_0 \cos(\chi - \chi_0). \tag{4.14}$$

Here, we neglected corrections to the frequency difference $(\Omega_1 - \Omega_2)$ of the order of ε. We also assumed times small compared to $-1/\text{Tr}_{1,2}$. The dimensionless factors Δ_0 and χ_0 are both of the order of 1. They are determined by the matrix elements of $\overleftrightarrow{M}_{1,2}$ and the initial conditions of the oscillation. Equation (4.14) is the equation of motion of a driven pendulum. The solution is well known: The average value of $d\chi/dt$ is nonzero as long as the absolute value of $(\Omega_1 - \Omega_2)$ exceeds the absolute value of $\varepsilon\Delta_0$. This means that two oscillations are not synchronized. At $|\Omega_1 - \Omega_2| = |\varepsilon\Delta_0|$, there is an infinite-period bifurcation below where the average value of $d\chi/dt$ goes zero. Beyond this point, the two oscillations are synchronized. At the transition point J_{ee}^{coup} is comparable to J_{ee}. In general, if the coupled networks are not synchronized, then the superposition of oscillations at different frequencies produces a noisy signal in the up-state potential. Synchronization of the up-state oscillations through a Kuramoto-type transition [41] suppresses this noise, but it would require the long-range matrix elements coupling the two networks, such as J_{ee}^{coup}, to be comparable to the short-range matrix elements, such as J_{ee}.

V. CONCLUSIONS

In summary, we have proposed a set of simple dynamical system descriptions for the UDS oscillations that combines synchronicity with up-state deterministic noise. The model appears to capture qualitatively the features of UDS oscillations listed in the Introduction. According to this model, the UDS oscillations are in near proximity to a partial synchronization transition characterized by pronounced deterministic noise, closely resembling the phase transition of statistical physics. The equations are sufficiently simple that they allow for an analytical treatment. We are currently carrying experimental studies of the cortex under conditions of gradual awakening to test the model quantitatively. While adaptation can get contributions from both synaptic and cellular sources, our hypothesis is that it is the dendritic mechanism that is more relevant for the up-down transitions. Since each dendrite gets inputs from hundreds of synapses, our current model, based on the average activity of neurons, is likely to work even when a network of spiking neurons is considered, which will be discussed elsewhere. In a recent study, Sussillo *et al.* [42] have shown that short-term plasticity of synapses can stabilize the

activity of a network. On the other hand, a recent study by Holcman and Tsodyks [35] showed that synaptic depression could generate slow oscillations. Thus, the behavior of large networks of spiking neurons can be quite complex and can depend on the parameter range. To our knowledge, no prior study has shown the emergence of reliable, bistable oscillations in a neuronal network.

Important aspects of the proposed theory are consistent with existing theoretical descriptions. The effects of competition between excitatory and inhibitory neurons have been extensively investigated for networks of point model neurons without adaptation. van Vreeswijk and Sompolinsky [43] showed that a finely balanced competition between excitatory and inhibitory neurons can produce a form of deterministic chaos with statistical features similar to those reported in actual neural circuits. Next, Holcman and Tsodyks proposed that UDS oscillations are governed by an oscillatory bistable system of the form discussed in Sec. III. However, in their case the up-state activity was generated by imposed network noise [35]. Finally, a large-scale numerical study of the up states by Millman *et al*. [44] of fully modeled neurons reported that up-state dynamics is characterized by saddle-node bifurcations, and that the competition between excitatory and inhibitory neurons generated spatially distributed states of self-organized criticality. The key differences between the present model an existing theories is (i) the key role of nonuniform network geometry and (ii) the introduction of DFSA.

As mentioned, the precise nature of up-state adaptation still has not been completely determined. The SFA process itself is best understood for the case of *somatic* adaptation [38,45–47]. This adaptation of the responsiveness of an excitatory cell occurs through calcium-activated potassium currents. Prolonged activation of an excitatory neuron produces an accumulation of Ca^{2+} in the cell body, which in turn activates the potassium conductance that reduces the neurons' ability to spike. Notably, the characteristic RC time scale of the membrane potential (of the order of milliseconds) is much shorter than the time scale for SFA (of the order of seconds). However, during one up state, cells fire at most a few action potentials, so it is not likely that this somatic SFA could set the duration of the up states. As mentioned, our work is based on Ref. [7] and the hypothesis [33–36] that up states are terminated by *dendritic* SFA. Alternate mechanisms also could also generate SFA. For example, the glial cells that typically surround synapses could influence the amount of extrasynaptic neurotransmitter levels during an up state, thereby influencing the network excitability.

It is interesting to speculate on the implications of our description. Other biological systems described in terms of continuous Hopf bifurcations, such as the hair cells of the inner ear, are associated with enhanced sensitivity to external input. The up state would thus be in a state of increasing responsiveness to external input in the vicinity of a Hopf bifurcation as well as be capable of computational activity involving different groups of neurons. The role of the down state would be the termination of increasing levels of neural activity in the up state that are not related to a purposeful response to external input. It also is amusing to note the similarity between a description of weak coupling between groups of internally strongly coupled collectives of excitatory and inhibitory neurons and the popular "small-world" description proposed for neural networks. In the future we plan to examine the behavior of our model for different ways of linking the groups of neurons.

ACKNOWLEDGMENTS

M.R.M was supported by the NSF Career Award No. 0969034, NIH/CRCNS Grant No. 1-5R01MH092925-02, the Whitehall Foundation, and the W. M. Keck Foundation. R.B. thanks the NSF for support via DMR Grant No. 1006128. A.J.L. thanks the NSF for support via DMR Grant No. 0907212.

APPENDIX: UP-STATE FIXED POINT ANALYSIS

In this Appendix, we examine the pair of equations

$$\frac{dv_e}{dt} = -\frac{1}{\tau_e}v_e + N_e J_{ee}(c) r(v_e) + N_i J_{ei} r(v_i) \tag{A1}$$

and

$$\frac{dv_i}{dt} = -\frac{1}{\tau_i}v_i + N_i J_{ii} r(v_i) + N_e J_{ie} r(v_e) \tag{A2}$$

to obtain explicit expressions for the null clines of Fig. 5 in order to locate the up-state fixed point and for the oscillation frequency. We will do this by approximating the expression for the firing rate as follows. Around the up-state fixed point, with $v_{e,i} \sim v^*$, the factor $\exp[(v_{e,i} - v^*)/g_{e,i}]$ is of the order of 1, while it is small compared to the one near the equilibrium potential when $v_{e,i} \sim 0$. Expanding the expression for the firing rate in powers of $\exp[(v_{e,i} - v^*)/g_{e,i}]$ gives

$$\frac{r_m}{1 + \exp[-(v_{e,i} - v^*)/g_{e,i}]} \approx r_m\{\exp[(v_{e,i} - v^*)/g_{e,i}] + \cdots\}, \tag{A3}$$

where we neglect terms of the order of $\exp[2(v_{e,i} - v^*)/g_{e,i}]$ and higher. In this approximation, which should hold for potentials up to the firing threshold, Eqs. (A1) and (A2) take the form

$$\frac{dv_e}{dt} \approx -\frac{1}{\tau_e}v_e + N_e J_{ee}(c) r_m \exp[(v_e - v^*)/g_e] - N_i |J_{ei}| r_m \exp[(v_i - v^*)/g_i], \tag{A4}$$

$$\frac{dv_i}{dt} \approx -\frac{1}{\tau_i}v_i - N_i |J_{ii}| r_m \exp[(v_i - v^*)/g_i] + N_e J_{ie} r_m \exp[(v_e - v^*)/g_e]. \tag{A5}$$

Starting with Eq. (A5), the null cline $\frac{dv_i}{dt} = 0$ can be written in explicit form as

$$v_e(v_i) \approx v^* + g_e \ln\left[\left(\frac{1}{\tau_i}v_i + N_i |J_{ii}| r_m \times \exp[(v_i - v^*)/g_i]\right) \Big/ N_e J_{ie} r_m\right]. \tag{A6}$$

The argument of the logarithm increases monotonically as a function of v_i so $v_e(v_i)$ is a monotonically increasing function as well. Further below the firing threshold, when v_i is small compared to v^*, the second term of the argument is negligible compared to the first term. One may then neglect the second so that the equation for the null cline reduces to $v_e(v_i) \approx v^* + g_e \ln(v_i/\tau_i N_e J_{ie} r_m)$. This means that, conversely, the null

cline is an exponential function of v_e:

$$v_i(v_e) \approx \tau_i N_e J_{ie} r_m \exp[(v_e - v^*)/g_e]. \quad \text{(A7)}$$

Equation (A7), in fact, fails for negative potentials (i.e., the hyperpolarized state) when the argument of the logarithm approaches zero. If, on the other hand, the potential approaches the firing threshold, Eq. (A7) fails as well. In this regime, one can neglect the first term in the argument of the logarithm of Eq. (A5), which produces a linear relationship

$$v_e(v_i) \approx v^* + (g_e/g_i)(v_i - v^*) + g_e \ln(N_i|J_{ii}|/N_e J_{ie}). \quad \text{(A8)}$$

For our estimated values, the slope g_e/g_i of the null cline is about 5/2. The exponential regime can be seen in the $\frac{dv_i}{dt} = 0$ null clines of Figs. 5(a)–5(c) for potentials less than about 15 mV. A quasilinear regime is seen for larger potentials but the predicted slope is too high compared with Eq. (A8). This is of course to be expected since higher-order terms in $\exp[(v_{e,i} - v^*)/g_{e,i}]$ should not be neglected for potentials exceeding the firing threshold. We will use Eq. (A6) when discussing the fixed points that lie in the intermediate range somewhat below the firing threshold.

Next we turn to the null cline $\frac{dv_e}{dt} = 0$. Using the same steps as before, one obtains

$$v_i(v_e) \approx v^* + g_i \ln\left[\left(-\frac{1}{\tau_e}v_e + N_e J_{ee}(c) r_m \times \exp[(v_e - v^*)/g_e]\right) \Big/ N_i|J_{ei}|r_m\right]. \quad \text{(A9)}$$

The change in sign of the first term of the argument has important effects because the argument of the logarithm must be positive. There are two separate "branches" for which this is the case. First, for very small potentials, the first term inside the large parentheses is smaller than the second term, in which case the argument is positive. Next, for larger potentials the second term exceeds the first term, as in the previous case, and the argument is positive as well. In between the two branches, which are obvious in Figs. 5(b) and 5(c), there is no solution. It is also clear from Fig. 5 that, for the up-state fixed point, we must focus on the second branch. Keeping only the second term in Eq. (A9) gives a linear null cline:

$$v_i(v_e) \approx v^* + (g_i/g_e)(v_e - v^*) + g_i \ln[N_e J_{ee}(c)/N_i|J_{ei}|]. \quad \text{(A10)}$$

The slope (g_i/g_e) is of the order of 2/5. A quasilinear regime indeed can be seen in Fig. 5, with a slope slightly larger than 2/5. The linear approximation works well for higher potentials, but fails for smaller potentials when the argument of the logarithm approaches zero when the $v_i(v_e)$ null cline has a logarithmic singularity. The two logarithmic singularities are located at solutions of the equation $v_e = -g_e W(-\gamma_0)$, where $W(z)$ is the *Lambert function* [defined implicitly through $z = W(z)\exp W(z)$]. The quantity $\gamma_0 = [N_e J_{ee}(c)\tau_e r_m/g_e]\exp(-v^*/g_e)$ is dimensionless and small compared to one in the limit that $v^* \gg g_e$. The Lambert function is double valued for negative arguments larger than $-1/e$. Choose the W_{-1} branch: The other branch corresponds to a regime of small potentials. In the limit of small γ_0, one can approximate $W_{-1}(-x) \approx \ln x$. The location of the logarithmic singularity is then

$$v_e^+ = v^* - g_e \ln[N_e J_{ee}(c)\tau_e r_m/g_e]. \quad \text{(A11)}$$

One can (crudely) represent the null cline $\frac{dv_e}{dt} = 0$ by the linear relation Eq. (A9), but terminate this relation at a vertical line that mimics the singularity at $v_e = v_e^+$. Figures 5(b) and 5(c) show that the location of the logarithmic singularity actually marks the location of an unstable fixed point.

If we represent the null cline $\frac{dv_i}{dt} = 0$ by the exponential relation Eq. (A7), one finds that the up-state fixed point is given in terms of a Lambert function as $v_i^* = -g_i W(-\gamma_1)$. Here $\gamma_1 = [N_i\tau_i r_m J_{ie}|J_{ei}|/J_{ee}(c)g_i]\exp(-v^*/g_i)$ is again a small dimensionless parameter. Using the same approximation for the Lambert function as before gives

$$v_i^* - v^* = -g_i \ln[\tau_i r_m N_i J_{ie}|J_{ei}|/J_{ee}(c)g_i]. \quad \text{(A12)}$$

Using this in the linear relation for the null cline gives the other coordinate of the up-state fixed point,

$$v_e^* - v^* \approx -g_e \ln(\tau_i r_m N_e J_{ie}/g_i), \quad \text{(A13)}$$

which is the result quoted in the main text. This analysis is only valid as long as v_e exceeds the location of the unstable fixed point v_e^+ where there is a logarithmic singularity in the null cline. The condition for the two fixed points to fuse is found by equating the location of the singularity with that of the fixed point. This gives rise to a critical synaptic strength $J_{ee}^* \equiv (g_e\tau_i/\tau_e g_i)J_{ie}$ for excitatory neurons.

Finally, we turn to the fixed-point oscillations. From Eqs. (A4) and (A5) it follows that the matrix elements are

$$a_{11} \approx -\frac{1}{\tau_e} + N_e J_{ee}(c)(r_m/g_e)\exp[(v_e^* - v^*)/g_e], \quad \text{(A14)}$$

$$a_{12} \approx -N_i|J_{ei}|(r_m/g_i)\exp[(v_i - v^*)/g_i], \quad \text{(A15)}$$

$$a_{22} \approx -\frac{1}{\tau_i} - N_i|J_{ii}|(r_m/g_i)\exp[(v_i^* - v^*)/g_i], \quad \text{(A16)}$$

$$a_{21} \approx N_e J_{ie}(r_m/g_e)\exp[(v_e^* - v^*)/g_e]. \quad \text{(A17)}$$

Inserting the up-state fixed-point coordinates gives simple expressions for the matrix elements associated with small deviations from the fixed point:

$$a_{11} \approx -\frac{1}{\tau_e} + \frac{1}{\tau_i}\left(\frac{g_i}{g_e}\right)\frac{J_{ee}(c)}{J_{ie}}, \quad \text{(A18)}$$

$$a_{12} \approx -\frac{1}{\tau_i}\frac{J_{ee}(c)}{J_{ie}}, \quad \text{(A19)}$$

$$a_{22} \approx -\frac{1}{\tau_i} - \frac{1}{\tau_i}\frac{|J_{ii}|J_{ee}(c)}{J_{ie}|J_{ei}|}, \quad \text{(A20)}$$

$$a_{21} \approx \frac{1}{\tau_i}\left(\frac{g_i}{g_e}\right). \quad \text{(A21)}$$

In the main text we discussed that strong oscillatory behavior is possible only if the trace of the matrix is nearly zero. In terms of the matrix elements, the trace is given by

$$\mathrm{Tr} \approx -\frac{1}{\tau_e} - \frac{1}{\tau_i} + \frac{1}{\tau_i}\frac{J_{ee}(c)}{J_{ie}}\left[\left(\frac{g_i}{g_e}\right) - \frac{|J_{ii}|}{|J_{ei}|}\right]. \quad \text{(A22)}$$

Setting the trace to zero is possible only if inhibitory-inhibitory synaptic coupling is sufficiently weak compared to the coupling between inhibitory and excitatory neurons so that $\frac{|J_{ii}|}{|J_{ei}|} < (\frac{g_i}{g_e})$. Assuming that this holds, we must demand

that

$$\frac{J_{ee}(c)}{J_{ie}} \approx \left(\frac{\tau_i}{\tau_e}+1\right) \Big/ \left[\left(\frac{g_i}{g_e}\right) - \frac{|J_{ii}|}{|J_{ei}|}\right]. \tag{A23}$$

If this condition is not obeyed then the decay rate is the inverse of the trace. Assuming that the trace has been set to zero, the oscillation frequency $\Omega \approx \sqrt{(a_{11}a_{22} - a_{12}a_{21})}$ is

$$\Omega \approx \frac{1}{\tau_i}\sqrt{\left[\frac{\tau_i}{\tau_e} - \left(\frac{g_i}{g_e}\right)\frac{J_{ee}(c)}{J_{ie}}\right]\left(1 + \frac{|J_{ii}|J_{ee}(c)}{J_{ie}|J_{ei}|}\right) + \left(\frac{J_{ee}(c)}{J_{ie}}\right)\left(\frac{g_i}{g_e}\right)}. \tag{A24}$$

A particular simple case is when one can neglect inhibitory-inhibitory coupling ($J_{ii} = 0$) when

$$\Omega \approx \frac{1}{\sqrt{\tau_e \tau_i}}, \tag{A25}$$

as quoted in the main text.

[1] For an introduction to bifurcation theory, see Steven H. Strogatz, *Nonlinear Dynamics And Chaos: With Applications To Physics, Biology, Chemistry, And Engineering* (Westview Press, Cambridge, MA, 1994). We use its notation and terminology.

[2] For an overview, see E. M. Izhikevich, *Dynamical Systems in Neuroscience: The Geometry of Excitability and Bursting* (MIT Press, Cambridge, MA, 2007).

[3] G. Buzsaki, *Rhythms of the Brain* (Oxford University Press, New York, 2006).

[4] C. J. Wilson and Y. Kawaguchi, J. Neurosci. **16**, 2397 (1996).

[5] M. Steriade, A. Nunez, and F. J. Amzica, J. Neurosci. **13**, 3252 (1993).

[6] D. Plenz and S.T. Kitai, J. Neurosci. **18**, 266 (1998).

[7] M. V. Sanchez-Vives, L. G. Nowak, and D. A. McCormick, J. Neurosci. **20**, 4286 (2000).

[8] C. C. H. Petersen, T. T. G. Hahn, M. Mehta, A. Grinvald, and B. Sackmann, Proc. Natl. Acad. Sci USA **100**, 13638 (2003).

[9] Image from [http://www.wikipedia.org/wiki/Neuron].

[10] R. Cowan and C. Wilson, J. Neurophysiol. **71**, 17 (1994).

[11] M. V. Sanchez-Vives and D. A. McCormick, Nat. Neurosci. **3**, 1027 (2000).

[12] Y. Shu, A. Hausenstaub, and D. A. McCormick, Nature (London) **423**, 288 (2003).

[13] B. Haider, A. Durque, A. R. Hasenstaub, and D. A. McCormick, J. Neurosci. **26**, 4535 (2006).

[14] J. Anderson, I. Lampl, I. Reichova, M. Carandini, and D. Ferster, Nat. Neurosci. **3**, 617 (2000).

[15] B. Haider, A. Duque, A. R. Hasenstaub, Y. Yu, and D. A. McCormick, J. Neurophysiol. **97**, 4186 (2007).

[16] C. Curto, S. Sakata, S. Marguet, V. Itskov, and K. D. Harris, J. Neurosci. **29**, 10600 (2009).

[17] R. Stickgold, Nature (London) **437**, 1272 (2005).

[18] L. Marshall, H. Helgadottir, M. Molle, and J. Born, Nature (London) **444**, 610 (2006).

[19] T. T. Hahn, B. Sakman, and M. R. Mehta, Nat. Neurosci. **9**, 1359 (2006).

[20] T. Wolansky, E. Clement, S. Peters, and M. Palczak, J. Neurosci. **26**, 6213 (2006).

[21] Y. Isomura, A. Sirota, S. Ozen, S. Montgomeery, and K. Mizuseki, Neuron **52**, 871 (2006).

[22] D. Contreras and M. Steriade, J. Neurosci. **15**, 604 (1995).

[23] M. Molle, L. Marshall, S. Gais, and J. Born, J. Neurosci. **22**, 10941 (2002).

[24] F. P. Battaglia, G. R. Sutherland, and B. L. McNaughton, Learn. Mem. **11**, 694 (2004).

[25] M. Molle, O. Yeshenk, L. Marshall, S. J. Sara, and J. Born, J. Neurophysiol. **96**, 62 (2006).

[26] M. R. Mehta, Nat. Neurosci. **10**, 13 (2007).

[27] D. Ji and M. A. Wilson, Nat. Neurosci. **10**, 100 (2007).

[28] Z. Chen, S. Vijayan, R. Barbieri, M. A. Wilson, and E. N. Brown, Neural Comput. **21**, 1797 (2009).

[29] S. Tokdar, P. Xi, R. C. Kelly, and R. E. Kass, J. Comput. Neurosci. **29**, 203 (2010).

[30] M. V. Sanchez-Vives, M. Mattia, A. Compte, M. Perez-Zabalza, and M. Winogrard, J. Neurophysiol. **104**, 1314 (2010).

[31] T. T. Hahn, B. Sakmann, and M. R. Mehta, Proc. Natl. Acad. Sci. USA **104**, 5169 (2007).

[32] J. M. McFarland, T. T. G. Hahn, B. Sakmann, and M. R. Mehta, PLoS One **6**, e21606 (2011).

[33] M. V. Tsodyks and H. Markram, Proc. Natl. Acad. Sci. USA **94**, 719 (1997).

[34] R. W. Pace, D. D. Mackay, J. L. Feldman, and C. A. Del Negro, J. Physiol. London **580**, 485 (2007).

[35] D. Holcman and M. Tsodyks, PLoS Comput. Biol. **2**, 174 (2006).

[36] G. Fuhrmann, H. Markham, and M. Tsodyks, J. Neurophysiol. **88**, 761 (2002).

[37] D. J. Schwab, R. F. Bruinsma, J. L. Feldman, and A. J. Levine, Phys. Rev. E **82**, 051911 (2010).

[38] P. A. Schwartzkroin and C. E. Stafstrom, Science **210**, 1125 (1980).

[39] Meyer B. Jackson, *Molecular and Cellular Biophysics* (Cambridge University Press, Cambridge, UK, 2006).

[40] F. J. Harris, Proc. IEEE **66**, 51 (1978).

[41] Juan A. Acebrón, L. L. Bonilla, Pérez Vicente, J. Conrad, Félix Ritort, and Renato Spigler, Rev. Mod. Phys. **77**, 137 (2005).

[42] D. Sussillo, T. Toyoizumi, and W. Maass, J. Neurophysiol. **97**, 4079 (2007).

[43] C. van Vreeswijk and H. Sompolinsky, Neural Comput. **10**, 1321 (1998); Science **274**, 1724 (1996).

[44] D. Millman, S. Mihalas, A. Kirkwood, and E. Niebur, Nat. Phys. **6**, 801 (2010).

[45] B. E. Alger and R. A. Nicoll, Science **210**, 1122 (1980).

[46] J. R. Hotson and D. A. Prince, J. Neurophysiol. **43**, 409 (1980).

[47] Yu Shan, D. Huang, W. Singer, and D. Nikolić, Cereb. Cortex **18**, 2891 (2008).